

The 21 May 2003 Tsunami in the Western Mediterranean Sea: Statistical and Wavelet Analyses

MOHAMMAD HEIDARZADEH^{1,2} and KENJI SATAKE²

Abstract—We report the statistical and wavelet analyses of the 21 May 2003 tsunami produced by an M_w 6.8–6.9 thrust earthquake in the western Mediterranean Sea using 19 tide gauge records. The largest trough-to-crest wave height was 196 cm recorded at the Sant Antoni station in the lee of the incoming tsunami wave. Except at one station, the first wave was not the largest wave at all the analyzed stations, and the largest wave arrived several hours after the first arrival. In addition, the tsunami waves persisted for more than 1 day at most stations. As the spectra of coastal tide gauge stations are strongly influenced by topographic features, special care was taken here while interpreting the results of spectral and wavelet analysis. Our wavelet analysis shows that only a peak at around 23 min is persistent for long duration, and other peaks at 14, 30, 45, and 60 min appeared at short durations. The 23-min signal is possibly associated with the width of the source fault whereas the fault length contributed to the 45-min signal. Based on these dominant periods, the tsunami source dimensions are estimated as $95 \text{ km} \times 45 \text{ km}$. The statistical and wavelet analyses performed here provide some new insights into the characteristics of the tsunami that was generated and propagated in the western Mediterranean basin.

Key words: Mediterranean Sea, 21 May 2003 earthquake, tsunami, tide gauge data, statistical analysis, wavelet analysis, numerical modeling, tsunami energy.

1. Introduction

The Mediterranean Sea is among the tsunamigenic regions in the world, according to historic and archaeological records. The region is susceptible to different types of tsunamis, i.e., tectonic, landslide and volcanic tsunamis (SOLOVIEV, 1990). A catalog of the Mediterranean tsunamis documented by

ANTONOPOULOS (1990) contains 141 tsunami events between 1800 AD and 1981 AD. SOLOVIEV (1990) identified eighteen tsunamigenic zones inside the Mediterranean region and compiled a catalog of 300 events.

A tsunami occurred in the western Mediterranean Sea on 21 May 2003 at 18:44 GMT offshore the northern coast of Algeria (Fig. 1). The tsunami, produced by an M_w 6.8–6.9 thrust earthquake (MEGHRAOUI *et al.* 2004; DEVERCHERE *et al.* 2005), was observed on many coastal areas of the western Mediterranean Sea (ALASSET *et al.* 2006). Little or no damage was reported due to the tsunami in the near-field, i.e., the Algerian coast (AYADI *et al.* 2003). However, a wave height of almost 2 m (ALASSET *et al.* 2006) was observed in the Spanish Balearic Islands (e.g., Ibiza in Fig. 1), at the distance of about 300 km from the source causing some moderate damage.

The source mechanism and generation phase of this tsunami was studied by several authors (e.g., YELLES *et al.* 2004; DELOUIS *et al.* 2004). TINTI *et al.* (2005) modeled this tsunami as one of the tsunami hazard scenarios for the Mediterranean region while ALASSET *et al.* (2006) numerically modeled the tsunami and compared the modeling results with limited sea level observations. WANG and LIU (2005) studied this tsunami by numerical modeling and made efforts to constrain the tsunami source using available tide gauge data. The source mechanism proposed by WANG and LIU (2005) was capable of reproducing the tsunami waveform recorded at the Sant Antoni station. VICH and MONSERRAT (2009) studied the source spectrum of the tsunami. Field investigation of the tsunami on the French coast and numerical modeling was performed by SAHAL *et al.* (2009).

¹ Faculty of Civil and Environmental Engineering, Tarbiat Modares University, Chamran Highway, Pol-e-Gisha, P.O.Box: 14115-397, Tehran, Iran. E-mail: m.heidarzadeh@modares.ac.ir

² Earthquake Research Institute (ERI), University of Tokyo, Tokyo, Japan.

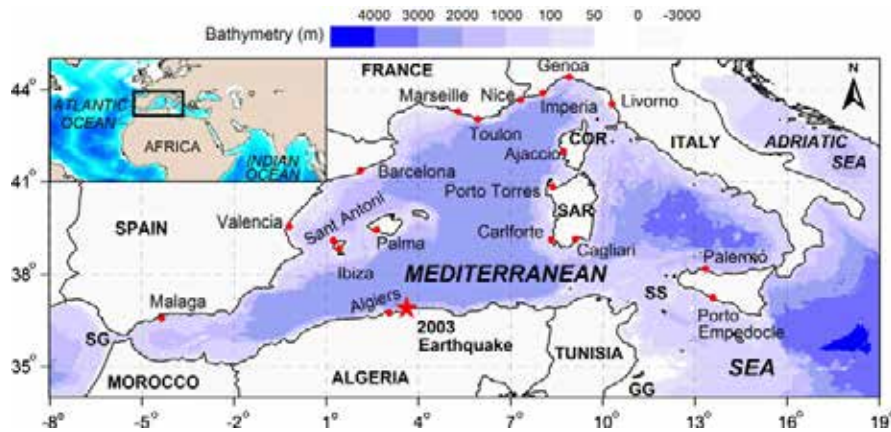


Figure 1

Geographical location of the study area showing the epicenter of the earthquake (red asterisk) and the tide gauge stations (red points). The inset shows the study area compared to the adjacent regions. Abbreviations are: SG Strait of Gibraltar; SS Strait of Sicily; GG Gulf of Gabes; COR Corsica, SAR Sardinia

This study is aimed at understanding the tsunami characteristics using tide-gauge data analysis along with wavelet analysis. Spectral analysis by VICH and MONSERRAT (2009) revealed that the major tsunami peak was around 21 min with two weaker peaks around 14 and 42 min. We used a larger number of tsunami waveforms than previous studies, and applied wavelet analysis to examine the temporal changes of the dominant spectral peaks. Our dataset includes 19 tide gauges whose locations cover almost the whole western Mediterranean Basin (Fig. 1).

2. Data

Sea level records for 19 tide gauge stations located across the Western Mediterranean Sea were analyzed. While several tide gauge records of the 21 May 2003 tsunami were used in previous studies, we extended the dataset in order to provide a relatively better understanding of this tsunami. These data were provided through different institutions, agencies and individuals including: UNESCO Intergovernmental Oceanographic Commission (Ioc, 2012), Puertos del Estado (Spain) available at: (<http://www.puertos.es/>), and the European Sea Level Service (ESEAS, 2012). The locations of the tide gauge stations are shown in Fig. 1 while their detailed information is summarized in Table 1. The distance to the source (Table 1) is

based on the assumption that the tsunami source was located at 3.60°E and 36.88°N and is calculated using a direct line connecting the tide gauge location to that of the tsunami source.

Due to the geographical locations of the tide stations, they can be classified into four groups: (1) Near-field stations (Ibiza, Palma, Sant Antoni, and Algiers); (2) western stations (Barcelona, Valencia, and Malaga); (3) northern stations (Toulon, Nice, Marseille, Ajaccio, Genoa, Imperia, and Livorno); and (4) eastern stations (Cagliari, Carloforte, Porto Empedocle, Palermo, and Porto Torres).

3. Waveform Analysis

The method used in this study for data processing is the same as the one used by RABINOVICH and THOMSON (2007) which includes the following steps:

1. Quality control of the data
2. Removing tide signal (de-tiding)
3. Removing low-frequency signals (high-pass filtering)
4. Tsunami detection and statistical analysis
5. Spectral analysis
6. Wavelet analysis (frequency-time analysis)

For estimating the tidal signal, the Tidal Analysis Software Kit (TASK) was employed (BELL *et al.* 2000). This package was developed at the Proudman Oceanographic Laboratory (POL) in the UK and has

Table 1
The tide gauges used in this study

No.	Sea level station	Country	Gauge type	Longitude	Latitude	Sampling rate (min)	Distance to the source (km)	Signal/noise ratio
1	Ibiza	Spain	Digital	01.44°E	38.91°N	5	331	8.1
2	Barcelona	Spain	Digital	02.16°E	41.35°N	5	524	4.0
3	Malaga	Spain	Digital	04.41°W	36.71°N	5	894	6.1
4	Valencia	Spain	Digital	00.33°W	39.46°N	5	525	4.6
5	Palma	Spain	Digital	02.62°E	39.55°N	1	317	7.2
6	Sant Antoni	Spain	Digital	01.30°E	38.97°N	2	347	10.2
7	Algiers	Algeria	Digital	03.00°E	36.75°N	10	80	–
8	Ajaccio	France	Digital	08.76°E	41.93°N	10	806	4.8
9	Marseille	France	Digital	05.36°E	43.29°N	10	742	1.9
10	Nice	France	Digital	07.28°E	43.69°N	10	864	3.7
11	Toulon	France	Digital	05.90°E	43.12°N	10	742	2.9
12	Cagliari	Italy	Digital	09.10°E	39.22°N	10	667	3.0
13	Imperia	Italy	Digital	08.03°E	43.88°N	10	925	3.6
14	Carloforte	Italy	Digital	08.33°E	39.15°N	10	586	4.2
15	Palermo	Italy	Digital	13.33°E	38.13°N	10	1,095	2.3
16	Livorno	Italy	Digital	10.30°E	43.55°N	10	1,056	2.6
17	Porto Torres	Italy	Digital	08.38°E	40.83°N	10	692	–
18	Porto Empedocle	Italy	Digital	13.52°E	37.28°N	10	1,109	2.8
19	Genoa	Italy	Digital	08.92°E	44.42°N	10	1,030	2.0

been widely used around the world for tidal analysis. It is a collection of Fortran procedures which provides full harmonic analysis of the observed tide gauge data. We used a 6-month dataset in each station for tide prediction in order to ensure high-quality tide predictions and to minimize possible associated errors. In our analysis, 55 major harmonic constituents were used to predict the tide. However, it should be added that due to some limitations, e.g., shortness of the time series' length, the TASK program is not able to remove very low-frequency signals from the tide gauge records. Therefore, to make the tsunami signal even clearer, we apply high-pass filtering to remove very low-frequency signals. The applied high-pass filter here is of the type of the Butterworth IIR digital filter (MATHWORKS, 2012) and the threshold frequency was chosen as 0.0002 Hz. It means that any signal having periods larger than 83.3 min will be removed.

Statistical details used for analysis of the tsunami signals include the tsunami arrival time, the sign of the first wave (either leading elevation or depression wave), the arrival time of the largest wave, trough-to-crest amplitude of the maximum wave, and the number of the maximum wave. The observed tsunami characteristics are presented in Table 2. We used a

combination of different criteria including comparison between observation and simulation, to estimate tsunami arrival times.

For numerical modeling of tsunami, we used the tsunami source proposed by WANG and LIU (2005) which includes: dip angle, 44°; slip angle, 71°; strike angle, 57°; top depth of fault, 10 km; fault length, 60 km; and fault width, 20 km. The analytical formulas by OKADA (1985) were employed to calculate the sea floor deformation due to the parent earthquake using the aforesaid seismic parameters. OKADA (1985) presented an analytical solution for the dislocation theory based on the models of elastic deformation on half-space. Thirty arc-second bathymetry grid provided through the GEBCO digital atlas (GEBCO_08 Grid, Version 20091120, <http://gebc0.net>) was used here. Figure 2 presents the snapshots of the tsunami propagation over the western Mediterranean Sea at 10 min intervals starting 20 min after the earthquake and ending 130 min later.

4. Frequency-Time (Wavelet) Analysis

Wavelet analysis or time–frequency analysis is a powerful tool to study the temporal variations of

Table 2

Statistical analysis of the tide-gauge records of the 21 May 2003 tsunami in the Western Mediterranean Sea

No.	Sea level station	First wave			Maximum wave			
		Arrival time (GMT) (Day/hh:mm)	Travel time (min)	Sign ^b	Arrival time (GMT) (Day/hh:mm)	Travel time (min)	Obs. max. wave height (cm) ^d	No. of the max. wave
1	Ibiza	21/19:25	40	(+)	21/21:24	160	59.3	5
2	Barcelona	21/20:00	75	(+)	21/23:10	266	43.0	9
3	Malaga	21/20:45	121	(+)	21/23:30	286	24.2	8
4	Valencia	21/20:14	90	(+)	22/01:55	431	66.6	18
5	Palma	21/19:36	52	(+)	21/21:37	173	115.7	6
6	Sant Antoni	21/19:52	68	(+)	21/20:12	88	196.0	2
7	Algiers	21/18:49	5	(-)	21/21:18	154	21.7	5
8	Ajaccio	21/20:00	76	(+)	21/23:30	286	12.4	7
9	Marseille ^c	21/20:12	88		22/09:20	876	04.9	8
10	Nice	21/20:12	88	(-)	21/21:00	136	12.4	3
11	Toulon	21/20:00	76	(+)	21/22:39	235	19.4	4
12	Cagliari	21/20:00	76	(+)	22/01:49	425	24.2	5
13	Imperia	21/20:30	106	(+)	22/00:20	336	05.8	5
14	Carloforte	21/19:58	72	(-)	21/20:00	75	28.0	1
15	Palermo ^c	21/20:54	130		22/03:30	526	06.6	-
16	Livorno	21/21:00	136	(+)	22/07:31	767	24.7	20
17	Porto Torres ^a	-	-	-	-	-	-	-
18	Porto Empedocle ^c	21/22:08	204		22/06:30	706	27.5	16
19	Genoa	21/20:40	116	(-)	22/04:49	605	12.2	15

^a No tsunami signal was identified

^b (-) and (+) represent leading depression and elevation waves, respectively

^c Due to high noise/signal ratio, arrival time is not identifiable on observed data. Thus it was calculated using simulation results

^d Maximum trough-to-crest wave height

time-dependent phenomena like tsunamis, storms and hurricanes. It is useful in tsunami research because tsunamis are highly energetic waves and thus the temporal variation of tsunami's energy is of importance to understand its behavior. The wavelet analysis shows the distribution of tsunami energy in different frequency bands (f) by passage of time (t). This is why it is sometimes known as the f - t analysis. In other words, the wavelet analysis shows that tsunami energy is concentrating in which period bands at different times. In fact, wavelet analysis can be considered as a complementary analysis for spectral analysis because the latter does not give the timing of each peak period band and its duration.

To address the problem of lack of timing in spectral analysis, a windowed Fourier transform was used as the first attempt in this context. In this method, the whole time series is divided into different overlapping segments and then the Fourier transform is applied on each

segment. However, it was discovered that this technique is inefficient and inaccurate as it is biased to window length (KAISER, 1994). Two main problems associated with the windowed Fourier transform are: (1) it applies a fixed window length which results in a poor time-frequency resolution, and (2) the windowed Fourier transform uses only a set of Sine and Cosine functions for its fitting procedure which are inefficient for catching all of the existing signals. But wavelet analysis lacks both shortcomings because, on the one hand, it employs a window width which is a function of frequency (varying windows) and, on the other hand, it applies a sophisticated function composed of a complex exponential equation modulated by a Gaussian function for its fitting procedure. This function is usually known as the *mother function* in wavelet literature.

One of the famous wavelet mother functions is the Morlet function [$\psi(t)$] which is given by the following equation (GOUPIILLAUD *et al.* 1984):

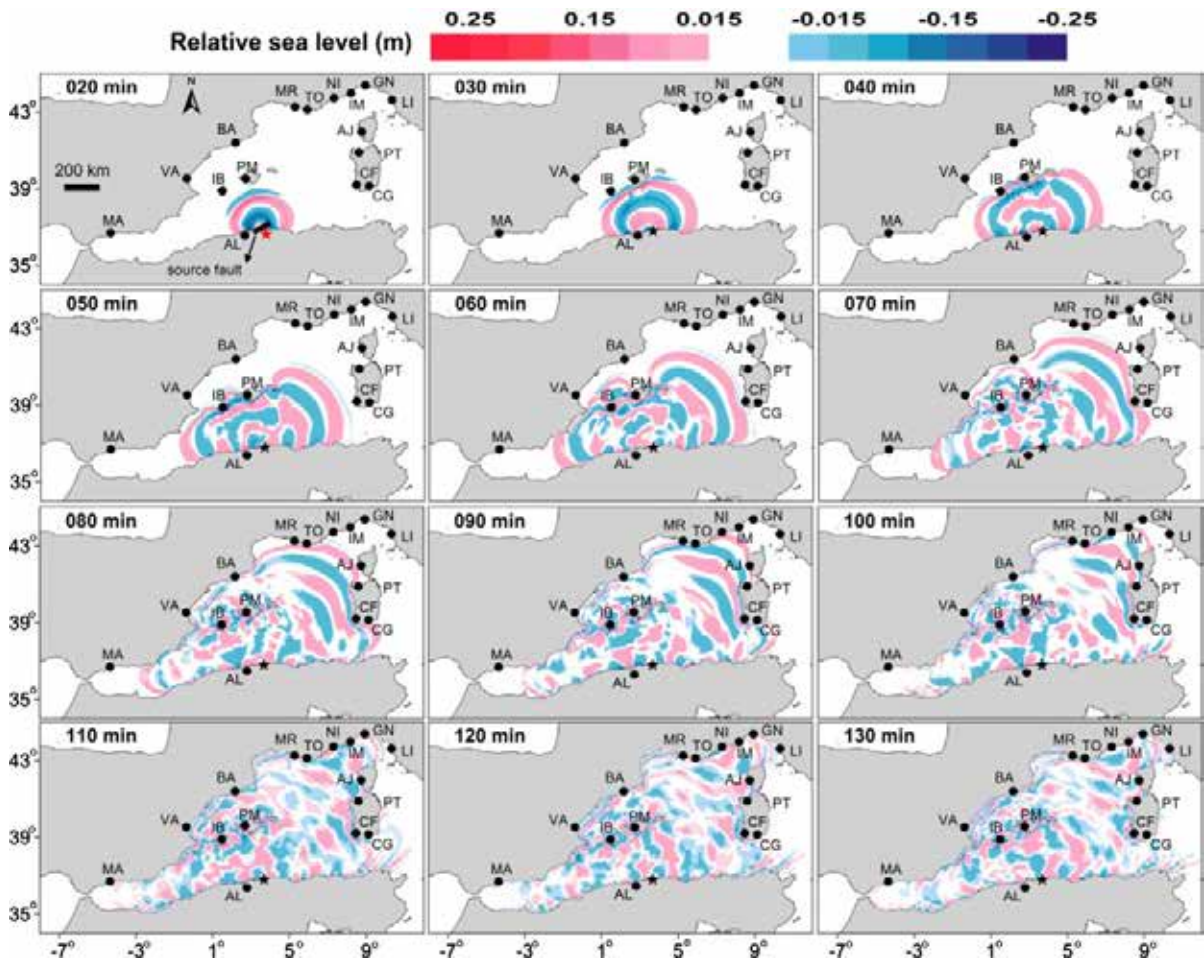


Figure 2

Snapshots of tsunami simulation at different times after the earthquake occurrence. The tsunami source proposed by WANG and LIU (2005) was used for tsunami simulation. The epicenter of the 21 May 2003 earthquake is shown by an asterisk. Abbreviations are: MA Malaga, VA Valencia, BA Barcelona, IB Ibiza, MR Marseille, TO Toulon, NI Nice, IM Imperia, GN Genoa, LI Livorno, AJ Ajaccio, PT Porto Torres, CF Carloforte, PM Palma, AL Algiers, and CG Cagliari

$$\psi(t) = \pi^{-1/4} e^{-1/2t^2} (1 + e^{-f_0^2} - 2e^{-3/4f_0^2})^{-1/2} (e^{jf_0 t} - e^{-1/2f_0^2}) \quad (1)$$

in which, j is the imaginary unit, f_0 is the central frequency of the wavelet function, and t is time. In the frequency domain, the Morlet function takes the following form:

$$\bar{\psi}(f) = \pi^{-1/4} (1 + e^{-f_0^2} - 2e^{-3/4f_0^2})^{-1/2} (e^{-1/2(f_0-f)^2} - e^{-1/2f_0^2} e^{-1/2f^2}) \quad (2)$$

in which, $\bar{\psi}(f)$ is the Fourier transform of $\psi(t)$. The Morlet wavelet mother function is used in this study

for our wavelet analysis. Here, we apply the wavelet analysis package developed by TORRENCE and COMPO (1998).

5. Results of Analyses

5.1. Near-Field Stations

Figure 3a presents the final tide gauge records corrected for tide and low-frequency signals for the four near-field stations of Algiers, Palma, Ibiza, and Sant Antoni. The tsunami signals are clear in all of these records. The arrival time of the first wave and

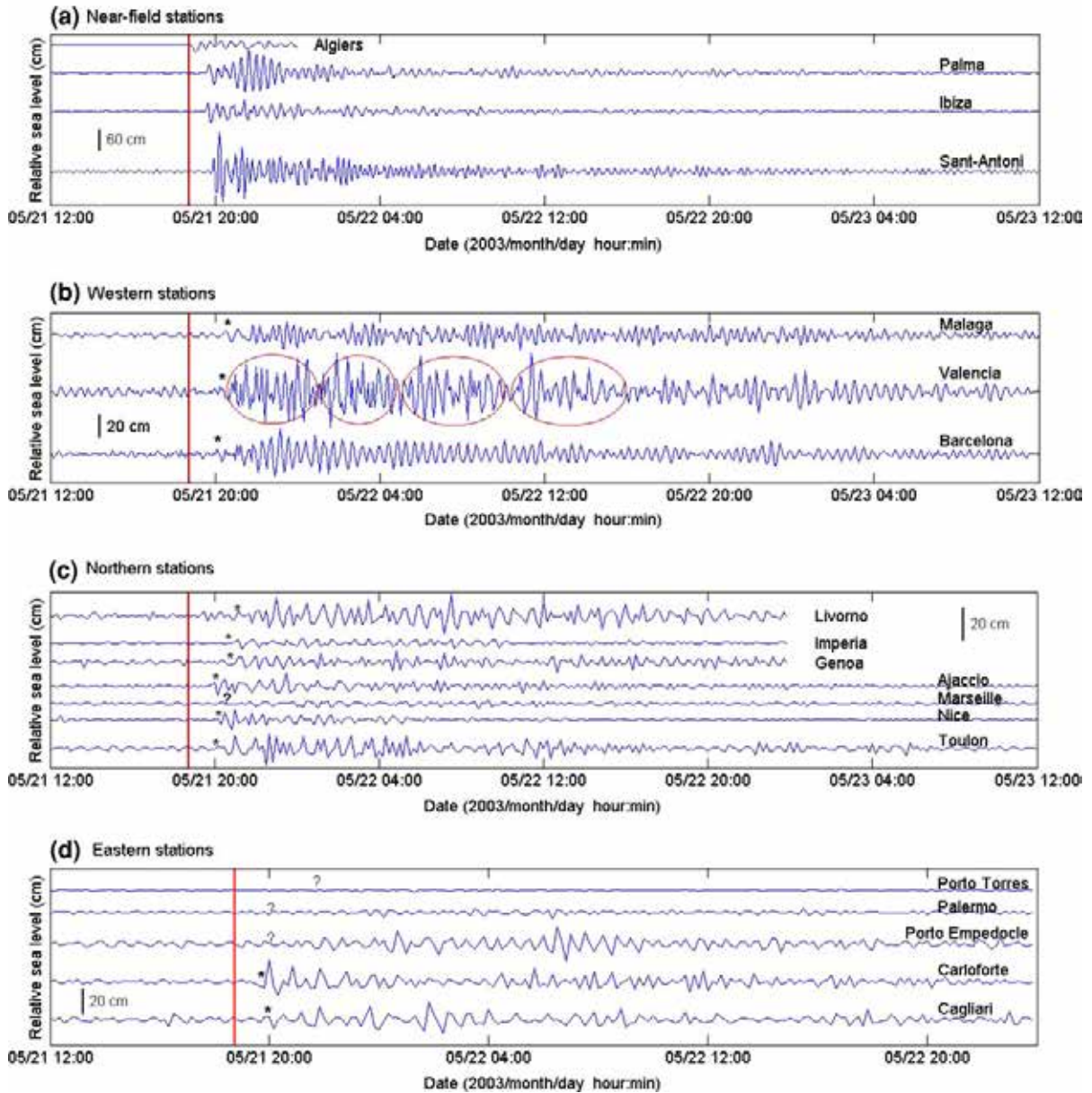


Figure 3

Time histories of the 21 May 2003 tsunami recorded at the near-field (a), the western (b), the northern (c) and the eastern (d) stations. Earthquake time is shown by the red vertical line. The asterisks show the tsunami arrival times. The red circles show distinct wave trains for the Valencia record. Question mark means that the tsunami arrival time cannot be identified

its sign (either depression or elevation wave) can be identified clearly. At the three stations of Palma, Ibiza, and Sant Antoni a first elevation wave was recorded whereas a leading depression wave was registered at the Algiers tide gauge. The first depression wave arrived at the Algiers station

5 min after the earthquake. However, numerical analysis shows that the first wave was of an elevation type in Algiers which seems reasonable. It is likely that the tide gauge record in Algiers is missing the first elevation wave due to its sampling interval of 10 min.

Among 19 tide gauge records examined in this study, the maximum trough-to-crest wave height was observed in Sant Antoni station with a value of 196 cm. This seems unusual because the Sant Antoni station is located in the lee of the incoming tsunami wave (Fig. 1). This can be attributed to the shape of the Ibiza Island which is nearly circular. As reported by ALASSET *et al.* (2006), the wave height of 196 cm is the result of the superposition of two waves arriving at the same time at the Sant Antoni station from different directions. The other tsunami that experienced the same phenomenon is the 12 December 1992 Flores tsunami in Indonesia in which the maximum runup of 7.2 m occurred on the nearly circular Island of Babi in the lee of the tsunami (SYNOLAKIS and OKAL, 2005). A similar observation was reported during the 30 December 2002 Stromboli tsunami in Southern Italy where the tsunami, generated at the north-west of the Stromboli Island, caused relatively strong effects at the opposite side of the island (TINTI *et al.* 2006).

The sixth, fifth, and second waves were the largest wave in Palma, Ibiza, and Sant Antoni stations, respectively. In Sant Antoni, the largest wave arrived 20 min later than the first tsunami wave, whereas it arrived 121 and 120 min after the first wave in Palma and Ibiza stations, respectively (Table 2).

Figure 3a shows that the tsunami signal is lasting for a relatively long time in all of the near-field stations and several distinct wave trains can be distinguished. In Palma and Sant Antoni, the tsunami waves are persisting until 23 May around 4:00 meaning a ringing time of more than 1 day. As defined by RABINOVICH and THOMSON (2007), ringing time means the duration of tsunami oscillations with significant wave heights. However, a shorter ringing time of about half a day is observed in Ibiza. These long ringing times and several wave trains can be partly attributed to the several reflections of tsunami waves from different coastal areas in this region like the northern coast of Algeria and the eastern coast of Spain. In fact, the western Mediterranean Basin behaves like a fairly enclosed basin and therefore any perturbation (e.g., tsunami generation) may result in persistent sloshing in this basin.

The result of the wavelet analysis for the Palma record (Fig. 4a) shows that tsunami energy is

distributed in three different bands of 23 min (circles in Fig. 4a), 42 min (rectangles A–C) and 65 min (rectangle A). The temporal variations of these periods (Fig. 4a) shows that, just after the tsunami arrival in Palma station, the period band of 65 min is governing but it switches to the period band of 22 min quickly and stays in this band until around 02:00 May 22 when the period of 42 min becomes the governing period. Again the period band of 21–25 min is governing from around 6:00 May 22 until the end of the tsunami oscillations. However, from both the wavelet plot and the mean spectrum presented in Fig. 4a, it is clear that most of the tsunami energy was concentrated at the period of around 23 min. The second and third peaks at Palma belong to the periods of 41 and 64 min, respectively. However, wavelet analysis shows that these two peaks (i.e., 41 and 64 min) are evanescent peaks (Fig. 4a). The two wave trains with energy content at 42-min period (rectangles B and C) occur 6 and 10 h after the earthquake.

The wavelet analysis for the Sant Antoni station (Fig. 4b) shows that the tsunami wave is characterized by almost monochromatic oscillation with a peak period around 20–25 min. Unlike Palma, almost no energy can be seen at the periods of around 45 or 60 min. The f - t plot of Sant Antoni is composed of several distinct lapses of high energy oscillations whose duration is smaller than those in the wavelet plot of the Palma record. Several gaps of no energy at the period band of 20–25 min can be seen on the wavelet plot of the Sant Antoni record shown by arrows in Fig. 4b. Lapses of high energy oscillations at the period band of around 20–25 min followed these gaps (circles in Fig. 4b). Tsunami waves at both stations of Sant Antoni and Palma persist until around 02:00 May 23 meaning a ringing time of around 30 h.

The wavelet analysis for the Ibiza record (Fig. 4c) reveals useful characteristics of the tsunami waves. Different wave trains can be distinguished which are shown by consecutive circles (Fig. 4c). These wave trains are clear in the time series of the Ibiza station too. According to this figure, the tsunami energy of almost all of these wave trains occurs at the period band of around 20–25 min. Figure 4c reveals that some of the tsunami energy is transferred to the two periods of around 14 and 42 min within the first few

hours after the earthquake generation (rectangles A and B in Fig. 4c). The energy at the period of 42 min (rectangle A) arrives relatively earlier than the one at the period of 14 min (rectangle B).

5.2. Western Stations

Figure 3b presents the high-pass filtered tidal residual for the three western stations. The signal-to-noise ratio is between 4 and 8.1 making the tsunami signal easily identifiable in all of these stations. However, the arrival times of tsunami in these stations are not as clear as those for the near-field stations. The background noise is high in Malaga record.

A first elevation wave was recorded in all of these stations. Among these stations, the maximum trough-to-crest wave height was observed in Valencia with a value of 66.6 cm (Table 2). It seems unusual that the largest wave in Valencia occurred 346 min after the arrival of the first wave (Table 2). Similar to the near-field stations, we observe that tsunami waves persist for more than 1.5 days in the western stations. Again, several wave trains are evident in these records. In all of the western stations, the arrival time of the maximum wave is more than three times longer than that of the first wave, and occurred several hours after the earthquake (Table 2). A look at Fig. 3a, b shows that the largest wave belongs to the first wave train in Ibiza, Barcelona, Sant Antoni, Palma and Malaga, but it belongs to the second wave train in Valencia. Distinct wave trains are shown by circles for the record of Valencia in Fig. 3b.

The $f-t$ plots for the western stations are shown in Fig. 4d. A clear peak around 20–23 min is dominating in all of them. However, two periods of 15 and 30 min are also high-energy content in Valencia. The tsunami energy is distributed in the band of 15–45 min in Malaga and Valencia stations whereas it is distributed on a relatively narrow band of 20–25 min in Barcelona.

Two distinct governing periods of around 23 and 45 min can be seen in Malaga (Fig. 4d). As shown by a rectangle on the Malaga wavelet plot in Fig. 4d, the period of around 45 min is dominating for a short time after the tsunami arrival (rectangle A). Again, this period band carries relatively high energy around

Figure 4

Results of the wavelet analyses for the sea level records of the near-field (a–c), the western (d), and the northern and eastern (e) stations. The color bar shows the $0.01 \times \text{Log}_2(\text{energy})$. The earthquake time is shown by the vertical thick line. RSL relative sea level

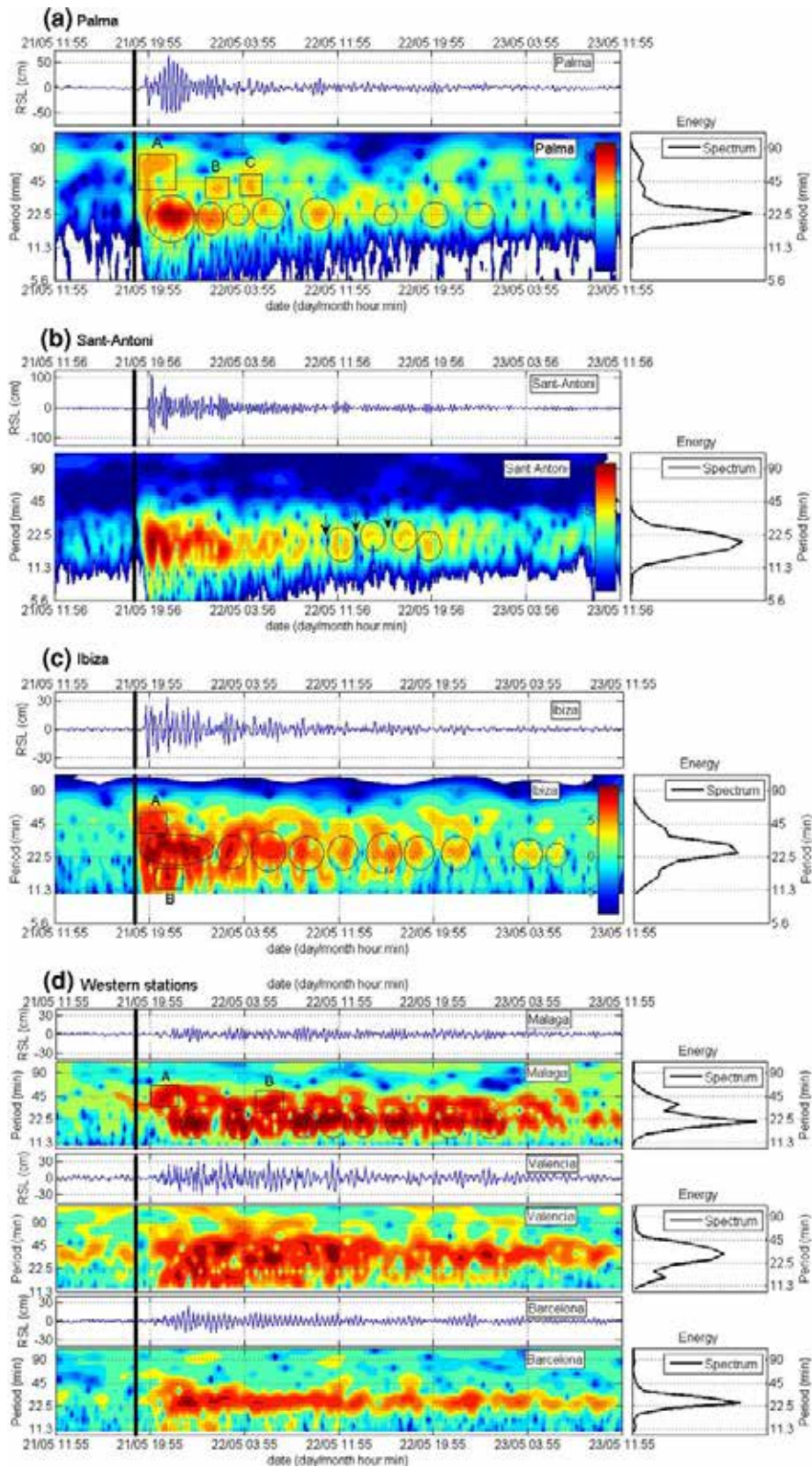
10 h after the earthquake (rectangle B). However, according to Fig. 4d, for almost the whole tsunami oscillation time, the governing period is around 22 min for the Malaga record. Similar to the Palma and Sant Antoni stations, the tsunami waves with significant energy are lasting for about 1.5 days in Malaga.

The wavelet plot for the Barcelona record is similar to that of the Sant Antoni one as both show an almost monochromatic oscillation with a peak period around 20–23 min. According to the wavelet plots for these two stations (Fig. 4b, d), no major deviations from the peak period can be seen in these stations during 2 days of tsunami oscillations. It seems that the sea level oscillations recorded in Barcelona and Sant Antoni are mostly affected by the tsunami source and that the effects of other phenomena like local harbor resonance are negligible in these stations. Although some other peaks are present in the spectrum of Barcelona like those at 36 and 12 min, the wavelet plot shows that these peaks are occurring for a relatively short time.

5.3. Northern Stations

Figure 3c presents the tide gauge records of the May 2003 Mediterranean tsunami in northern stations. The signal-to-noise ratio is between 1.9 and 4.8 in these stations (Table 1). According to Fig. 3c, the tsunami signal is identifiable in all of these stations. However, the signal is relatively weak in Marseille. The first arrival is not clear on the tsunami signals. Therefore, application of other criteria such as agreement between neighboring stations and comparison between observation and simulation is necessary. Using these criteria, the arrival times of the tsunami waves were determined and are shown with asterisks on Fig. 3c.

Distinct wave trains are evident in the records (Fig. 3c). Tsunami waves persist for more than a day in Ajaccio, Marseille, and Toulon, whereas it



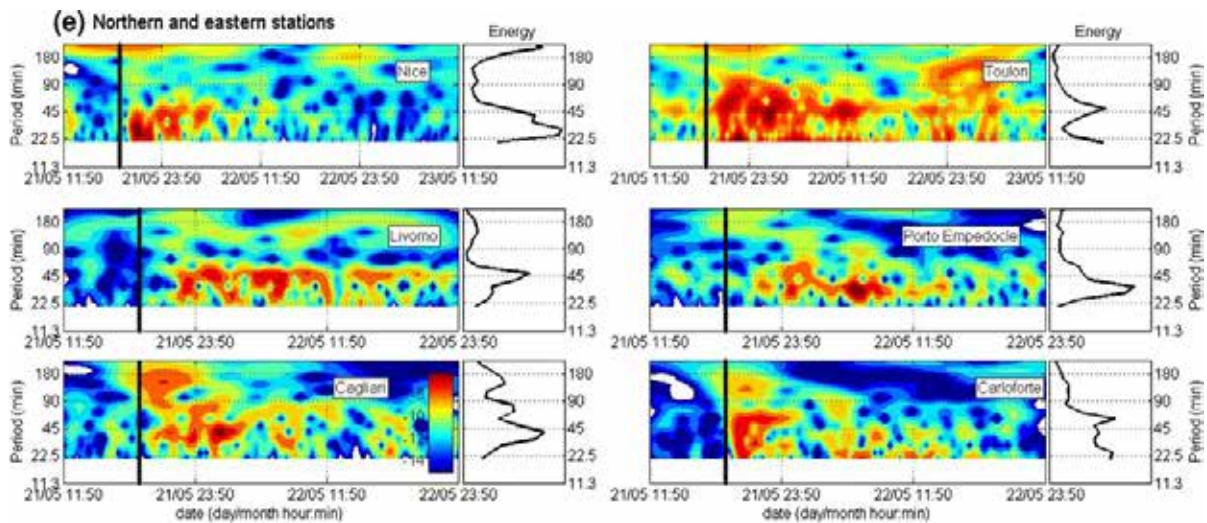


Figure 4
continued

disappears about half a day after the earthquake in Nice (Fig. 3c).

Generally, the amplitudes of the tide gauge records in the northern part of the western Mediterranean basin are considerably smaller than those for the stations located at the near-field and western parts of the basin. The maximum wave height is between 5.8 and 24.7 cm for the northern stations, whereas it is between 24.2 and 66.6 cm for the western ones, and between 59.3 and 196.0 cm for the near-field stations. This difference can be explained by the effect of the directivity of tsunami waves (BEN-MENAHEM and ROSENMAN 1972). For this tsunami it is evident that most of the tsunami's energy propagates towards the Balearic Islands (i.e., Ibiza, Palma, and Sant Antoni) and the western part of the western Mediterranean Basin. The alignment of the source fault is shown in Fig. 2-first panel.

Figure 4e presents the f - t plots for some of the northern stations (i.e., Nice, Toulon, and Livorno). In these stations, both 23- and 45-min signals are strong. In Nice, the 23-min signal is governing but in Livorno the 45-min signal is dominating. Both signals are almost of the same strength in Toulon. It seems that there is a connection between the dominant period of tsunami signal in a particular station and its location relative to the strike of the tsunami source fault. We have some discussion about this later in the paper.

5.4. Eastern Stations

Tide gauge records of the eastern stations are presented in Fig. 3d. No tsunami was recorded in Porto Torres. In other stations, the tsunami signal is identifiable although it is weak in Palermo. The first arrival of tsunami is clear enough in the two stations of Carloforte and Cagliari (Fig. 3d), whereas we were unable to determine the first arrival times of tsunami waves in Palermo and Porto Empedocle.

The background noise is relatively high in Porto Empedocle and Cagliari. Similar to the observations in the western and northern coasts, the generated oscillations due to the tsunami last for more than 1 day in most of the eastern stations, and several wave trains are evident in the records (Fig. 3d). No tsunami wave was recorded in the Porto Torres station (Fig. 3d). This is most likely due to its specific geographical location which sheltered the station from the incoming tsunami (Fig. 1).

Figure 4e presents the f - t plots for selected eastern stations. Among the examined tsunami records, the two periods of around 22 and 60 min are dominating in Carloforte. The energy is concentrated in a relatively long period band of 20–60 min within the first 2 hours of tsunami arrival in Carloforte (Fig. 4e). The global wavelet spectrum for Carloforte shows almost the same energy level for the period band of 20–60 min. In Porto Empedocle, the energy is mostly

concentrated at the period band of 20–45 min with a major peak at 30 min. In Cagliari, the peak period is 45 min. In all of the examined eastern stations, the first arriving waves at these stations have a period of around 45 min.

6. Discussions

Several factors are contributing to different spectral peaks observed in tide gauge records including local bathymetry and harbor resonance, regional bathymetry and shelf effect, global basin-wide effects and associated basin oscillations, and also the tsunami source effects. For example, the relatively monochromatic oscillations observed in Sant Antoni (Fig. 4b) and Barcelona (Fig. 4c) possibly can be attributed to the tsunami source whereas other factors such as harbor or basin oscillations seem to be contributing to the polychromatic oscillations observed in Valencia (Fig. 4d) and Cagliari (Fig. 4e).

Our study shows that there is a correlation between the observed spectral peaks and the location of the tide gauge station compared to the fault strike. Using theoretical spectral analysis, ABE (2006) found that the dominating period for the stations located along and normal to the fault strike are significantly affected by the fault length and width, respectively. Although it is already known that three main tsunami periods of the 2003 event are 14, 21 and 42 min (VICH and MONSERRAT 2009), our wavelet analysis shows the timing of the different signals. The first tsunami waves arriving in Malaga have a period of around 45 min whereas the first waves contain a 23-min signal in Ibiza. The periods of the first tsunami waves arriving at the tide gauge stations are shown in Fig. 5a while Fig. 5b presents the dominating periods of the tsunami waves during the whole tsunami oscillations in some stations. These periods are clear in wavelet analysis (Fig. 4). Based on Fig. 5a, it seems that the period of the first tsunami signal is a function of the location of the tide gauge station compared to the strike of the source fault. For the stations located perpendicular to the fault strike (e.g., Ibiza and Palma in Fig. 5a), the first waves have a period of around 23 min. And for the stations located along the fault strike (e.g., Malaga and

Cagliari), the period of the first wave is around 45 min. It should be added that for the latter stations (e.g., Malaga), the 23-min signal is again prevailing by passage of time (Fig. 5b).

Figures 4 and 5b reveal that the tsunami signal with the period of around 23 min is the most powerful signal of the tsunami because it is rather strong in all of the examined stations. Since most of the tsunami energy occurs in the direction normal to the fault strike based on the directivity effect and knowing that the tsunami signal in this direction is dictated by the fault width, it may be concluded that the 23-min signal is associated with the width of the source fault. Usually fault length has a little contribution to the tsunami spectra. The 45-min signal, which is the first wave arriving in Malaga and some eastern stations (Fig. 5a) and also is the dominating signal in few stations (Fig. 5b), is possibly associated with the fault length.

Efforts were made by some authors to estimate the dimensions of a tsunami source (length and width) using dominant tsunami periods (e.g., RABINOVICH and THOMSON 2007; ABE 2006). The calculations were made using the hydrodynamic equation relating phase velocity of tsunami at the source area with its dominant periods:

$$\lambda = T\sqrt{gh} \quad (3)$$

where λ is tsunami wavelength in meters, g is the gravitational acceleration in m/s^2 , h is ocean water depth at the source area in meters, and T is the dominant period of tsunami in seconds. $C = \sqrt{gh}$ is the phase velocity of tsunami. The tsunami source length (L) or width (W) can be estimated from the tsunami wavelengths in the corresponding direction, i.e., λ_L and λ_W , which are the tsunami wavelengths in the directions along and normal to the fault strike, respectively. It is assumed that tsunami wavelengths are up to twice the length or width of the source fault, i.e., $\lambda_L \sim 2L$ and $\lambda_W \sim 2W$. It is clear that the estimation of tsunami source dimensions using Eq. (3) is rather ad hoc because, for example, by increasing the water depth at the tsunami source (h) by a factor of 2, the wavelength (λ) will increase by a factor of 1.4. This shows that the estimations made by Eq. (3) are sensitive to water depth, and, hence, this equation should be applied cautiously. For the 21 May 2003

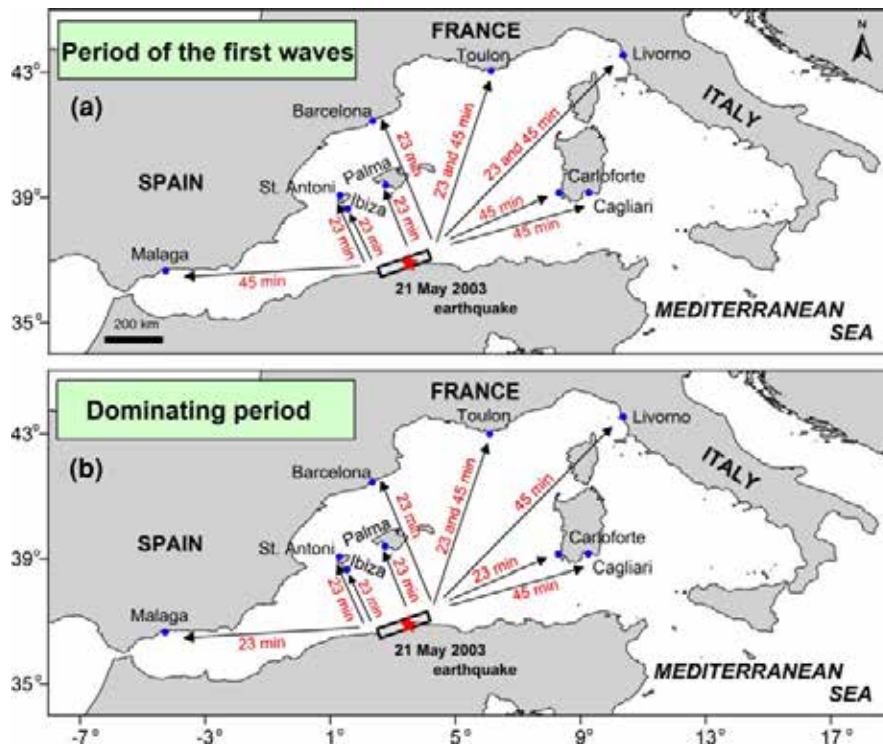


Figure 5

The western Mediterranean basin along with the location of the 21 May 2003 earthquake (the *asterisk*) and the locations of some tide gauge stations in the region (*filled circles*). The *numbers on the arrows* show the period of the first tsunami waves arriving in each tide gauge station (*top panel*) and the dominating tsunami periods during the whole tsunami oscillations (*bottom panel*). The *rectangle* is an approximate representative of the tsunami source fault

tsunami, the water depth at the source is in the range of 0–1,000 m. By assuming an average water depth of 500 m and using two dominant periods of 22 and 45 min, application of Eq. (3) yields two wavelength of 90 km (λ_W) and 190 km (λ_L). Therefore, using our spectral and wavelet analysis, the source length and width of the 21 May 2003 tsunami are estimated as 95 and 45 km, respectively. These values are close to the source dimensions proposed by WANG and LIU (2005) which is around 100 km \times 40 km (see Fig. 9 in WANG and LIU, 2005).

According to wavelet plots in Fig. 4, different lapses of high-energy sea level oscillations can be observed which are shown by circles and rectangles in this figure. The physical origin of each lapse may be distinguished from their periods in the wavelet plot. For example, for the Palma record (Fig. 4a), the wave trains which occur several hours after the earthquake and have a period of around 23 min (circles) are possibly the reflected waves from

different coasts in the region which still carry the source signal.

Our wavelet analysis also shows that some peaks in the tsunami spectra are evanescent peaks. Examples are the 60- and 45-min signals in Palma and Ibiza stations, respectively. This is a useful piece of information letting us understand tsunami characteristics. For example, the first signal in Malaga is the 45-min one but is lasts less than an hour and afterwards the governing signal will be the 23-min one for a long time. In fact, it shows that the most powerful signal of the tsunami (i.e., the 23-min signal associated with the fault width) arrived in this station with around 1 h delay.

It was previously discussed that the observation of the maximum trough-to-crest wave height at the Sant Antoni station in the lee of the incoming tsunami can be attributed to the superposition of two waves arriving at the same time from different directions (ALASSET *et al.* 2006). However, it seems that the resonance of the Sant Antoni harbor due to the

incoming tsunami contributed to this unusual observation too. According to the spectral study by VICH and MONSERRAT (2009), the peak period of the background signal at this harbor is around 18 min which is close to the main period of the tsunami signal (i.e., 21 min), and hence harbor resonance due to the incoming tsunami wave is possible.

7. Conclusions

The 21 May 2003 tsunami in the western Mediterranean Sea was analyzed using 19 tide gauge records of this tsunami. While taking into account that spectra of coastal stations are strongly influenced by topographic features, and special care should be given for interpreting them, the main findings are:

1. The largest recorded trough-to-crest wave height was 196 cm which was recorded at the Sant Antoni station in the lee of the incoming tsunami wave.
2. Several wave trains are observable in most of the tide gauge records, and hence the duration of the tsunami wave with significant wave height is more than 1 day for most of the sea level records.
3. The largest tsunami wave was the third, fourth or later wave and arrived several hours after the first arrival of the tsunami in most of the examined stations. And in some cases, the largest wave belonged to the second wave train.
4. The main tsunami signal has a period of around 23 min which is possibly associated with the width of the source fault. It is likely that the fault length contributed to the tsunami signal with a period of around 45 min. We estimate the length and width of the tsunami source fault as 95 and 45 km, respectively, using these dominant periods.
5. It was observed that the tsunami spectral peaks at 30, 45 and 60 min are evanescent peaks.
6. Wavelet plots reveal that high-energy oscillations persist around 1.5 days in the western Mediterranean basin.

Acknowledgments

We thank the following institutions for making available the data used in this study: UNESCO

Intergovernmental Oceanographic Commission, Puertos del Estado (Spain), and the European Sea Level Service. We are sincerely grateful to Dr. Belen Martin-Miguez (Centro Tecnológico del Mar Fundación CETMAR, Vigo, Spain) for providing the tide gauge data for Palma and Sant Antoni stations. We thank Stefano Corsini from the Institute for Environmental Protection and Research, Rome, Italy for providing the Italian tide gauge records. The first author is sincerely grateful to Prof. Michael Tsimplis for holding useful discussions with him about the Mediterranean tsunamis. We sincerely thank Prof. Alexander Rabinovich (the editor) and two anonymous reviewers for their detailed reviews of this article.

REFERENCES

- ABE, K. (2006). *Dominant periods of the 2004 Sumatra tsunami and the estimated source size*, Earth Planets Space, 58:217–221.
- ALASSET, P.-J., HEBERT, H., MAOUCHE, S., CALBINI, V., and MEGHRAOUI, M. (2006). *The tsunami induced by the 2003 Zemmouri earthquake (MW = 6.9, Algeria): modeling and results*, Geophys. J. Int., 166:213–226.
- ANTONOPOULOS, J. (1990). *Data for investigating tsunami activity in the Mediterranean Sea*, Sci. Tsunami Hazards, 8:39–52.
- AYADI, A., MAOUCHE, S., HARBI, A., and MEGHRAOUI, M. (2003). *Strong Algerian earthquake strikes near capital city*, Eos Trans. AGU, 84(50):561–568.
- BELL, C., VASSIE, J.M., and WOODWORTH, P.L. (2000). *POL/PSMSL Tidal Analysis Software Kit 2000 (TASK-2000)*, Permanent Service for Mean Sea Level. CCMS Proudman Oceanographic Laboratory, UK, 22p.
- BEN-MENAHEN, A., and ROSENMAN, M. (1972). *Amplitude patterns of tsunami waves from submarine earthquakes*, J. Geophys. Res., 77:3097–3128.
- DELOUIS, B., VALLEE, M., MEGHRAOUI, M., CALAIS, E., MAOUCHE, S., LAMMALI, K., MAHSAS, A., BRIOLE, P., BENHAMOUDA, F., and YELLES, K. (2004). *Slip distribution of the 2003 Boumerdes-Zemmouri earthquake, Algeria, from teleseismic, GPS, and coastal uplift data*, Geophys. Res. Lett., 31, L18607.
- DEVERCHERE, J., YELLES, K., DOMZIG, A., MERCIER DE LEPINAY, B., BOUILLIN, J.-P., GAULLIER, V., BRACENE, R., CALAIS, E., SAVOYE, B., KHERROUBI, A., LE ROY, P., PAUC, H., and DAN, G. (2005). *Active thrust faulting offshore Boumerdes, Algeria, and its relations to the 2003 Mw 6.9 earthquake*, Geophys. Res. Lett., 32, L04311.
- ESEAS (2012). *The European Sea-Level Service*, Available at <http://www.es seas.org/>.
- GOUPILLAUD, P., GROSSMAN, A., and MORLET, J. (1984). *Cycle-Octave and related transforms in seismic signal analysis*, Geophysical Research Letters, 11:85–102.
- IOC (2012). *Sea Level Station Monitoring Facility*, at: <http://www.ioc-sealevelmonitoring.org/map.php>.
- KAISER, G. (1994). *A Friendly Guide to Wavelets*. Birkhäuser, 300 p.

- MATHWORKS (2012). *MATLAB user manual*, The Math Works Inc., MA, USA, 282 p.
- MEGHRAOUI, M., MAUCHE, S., CHEMAA, B., CAKIR, Z., AOUDIA, A., HARBI, A., ALASSET, P.-J., AYADI, A., BOUHADAD, Y., and BENHAMOUDA, F. (2004). *Coastal uplift and thrust faulting associated with the $M_w = 6.8$ Zemmouri (Algeria) earthquake of 21 May, 2003*, *Geophys. Res. Lett.*, *31*, L19605.
- OKADA Y. (1985). *Surface deformation due to shear and tensile faults in a half-space*, *Bull. Seismol. Soc. Am.*, *75*(4): 1135–1154.
- RABINOVICH, A.B., and THOMSON, R.E. (2007). *The 26 December 2004 Sumatra Tsunami: Analysis of Tide Gauge Data from the World Ocean Part 1. Indian Ocean and South Africa*, *Pure Appl. Geophys.*, *164*:261–308.
- SAHAL, A., ROGER, J., ALLGEYER, S., LEMAIRE, B., HEBERT, H., SCHINDELE, F., and LAVIGNE, F. (2009). *The tsunami triggered by the 21 May 2003 Boumerdes-Zemmouri (Algeria) earthquake: field investigations on the French Mediterranean coast and tsunami modeling*, *Nat. Hazards Earth Syst. Sci.*, *9*:1823–1834.
- SOLOVIEV, S.L. (1990). *Tsunamigenic zones in the Mediterranean Sea*, *Natural Hazards* *3*:183–202.
- SYNOLAKIS, C.E., and OKAL, E.A. (2005). *1992-2002: perspective on a decade of post-tsunami surveys*, in: *Tsunami* (K. SATAKE, ed.), *Adv. Nat. Technol. Hazards Res.*, *23*:1–30.
- TINTI, S., ARMIGLIATO, A., PAGNONI, G., and ZANIBONI, F. (2005). *Scenarios of Giant Tsunamis of Tectonic origin in the Mediterranean*, *ISET Journal of Earthquake Technology*, *42*(4):171-188.
- TINTI, S., PAGNONI, G., and ZANIBONI, F. (2006). *The landslides and tsunamis of the 30th of December 2002 in Stromboli analysed through numerical simulations*, *Bull. Volcanol.*, *68*:462–479.
- TORRENCE, C., and COMPO, G.P. (1998). *A practical guide to wavelet analysis*, *B. Amer. Meteorol. Soc.*, *79*(1):61–78.
- VICH, M.M., and MONSERRAT, S. (2009). *Source spectrum for the Algerian tsunami of 21 May 2003 estimated from coastal tide gauge data*, *Geophys. Res. Lett.*, *36*, L20610.
- WANG, X., and LIU, P. L.-F. (2005). *A Numerical Investigation of Boumerdes-Zemmouri (Algeria) Earthquake and Tsunami*, *Comput Model Eng Sci.*, *10*:171–183.
- YELLES, K., LAMMALI, K., and MAHSAS, A. (2004). *Coseismic deformation of the May 21st, 2003, $M_w = 6.8$ Boumerdes earthquake, Algeria, from GPS measurements*, *Geophys. Res. Lett.*, *31*, L13610.

(Received January 15, 2012, revised May 23, 2012, accepted May 24, 2012, Published online July 7, 2012)